University of Reading
Department of Meteorology

Vertical Coordinates over Orography

By Matthew Rout

Supervised by Hilary Weller

March 12th 2014

Submitted in partial fulfillment of the requirements of the degree of Bachelor of Science, Meteorology at the University of Reading.

Abstract

Vertical Coordinates over Orography

Steep orography in high resolution Numerical Weather Prediction (NWP) models can lead to significant errors calculating horizontal pressure gradients (***Klemp 2011***). There are two main ways in which the atmosphere is modelled over orography; terrain following coordinates where mesh layers follow the orography, and cut cells where the mesh layers are horizontal and intersect the orography. Horizontal pressure gradients can be calculated more accurately with cut cells, which can lead to more accurate simulation of the equations of motion (***Steppeler et al. 2013***). The two methods are compared using a test case with orography described in ***Schär et al. 2002***, a case which was originally created to demonstrate the benefits of smooth terrain following coordinates. It is a case which has not been used previously with cut cells, since the orography is low in comparison the mesh resolution meaning that cut cells will not clearly be so beneficial.

A numerical model is used which can simulate the compressible Euler equations on any mesh. A variety of methods for representing orography at various resolutions are compared for the ***Schär et al. 2002*** test case. These are terrain following, cut cells, step orography, local refinement and cut cell meshes with mesh relaxation. Two factors which can contribute to reduced accuracy are non-orthorgonality and skewness are explored for each mesh.

Adding local refinement is the most pleasing of results as it allows a downdraft to become visible close to the orography, something which does not appear in low resolutions. This is particularly useful because it means that the broad scale resolution can stay low, with just a small part of the mesh at the bottom of the domain having a higher resolution, which is much more efficient than a broad scale high resolution.

Contents

Table of Contents

Introduction

1.1 Motivation

Steep orography in high resolution Numerical Weather Prediction (NWP) models can lead to significant errors calculating horizontal pressure gradients (***Klemp 2011***). The most common way to model over orography is to use terrain following coordinates, (***Leuenberger 2001***), a method which will be described in detail in section 1.2, in which mesh layers follow the orography. Another technique is to use z coordinates with cut cells (***Ingram et al. 2003***), described in section 1.3, where instead of following the orography, the mesh layers are horizontal and intersect with the orography.

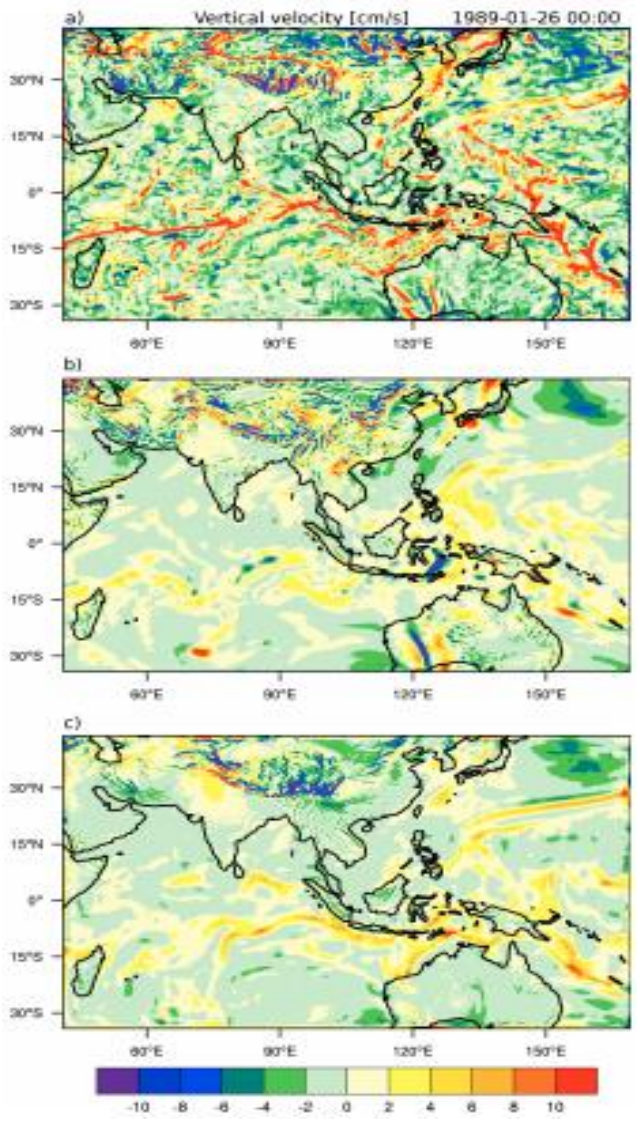

Figure 1 Image from Steppeler et al 2013 showing a) A terrain following Vertical Velocity 5-day forecast b) An analysis of vertical velocity after 5 days c) A Cut Cells Vertical Velocity 5 day forecast

Horizontal pressure gradients can be calculated more accurately with cut cells, which can lead to more accurate simulation of the equations of motion. An example of this is shown in figure 1 (***Steppeler et al 2013***) which shows 5 day vertical velocity (w) forecasts using cut cells and terrain following coordinates then compares them to the analysis of the conditions after the 5 days. It shows that the terrain following forecast overestimates the magnitude of the vertical velocities over the Himalayan regions and also in regions within the Indian and Pacific Oceans, whereas the cut cells version fits in much more closely to the analysis after 5 days. However there are some disadvantages to cut cells. For efficiency, atmospheric model vertical resolution decreases with height.

This is so the boundary layer can be modelled in the greatest detail, as it is one of the most complex features of the atmosphere. However when you implement orography into the mesh using cut cells, the top of the orography can be within the coarser resolution. This means that the boundary layer at the top of the orography is not modelled as accurately as the bottom. In this report I will investigate some alternative approaches such as using local resolution at the top of mountains and orthogonal, terrain following layers. A further problem with cut cells arises when cells very close to the orography become very small, leading to instability. This problem is explored in detail in section 1.6.

In this report I aim to review the literature on cut cell and terrain following modelling of the flow around orography; subject cut cell techniques to a test case for which they are clearly not well suited and add local refinement of the orography.

1.2 Terrain Following Coordinates

***Gal-Chen and Sommerville 1975*,** introduced us with what is known to us today as the Basic Terrain Following coordinate transformation. It is described using the following equation:

$$z = (z_T - h)\frac{\eta}{z_T} + h$$
$$= \eta + \left(1 - \frac{\eta}{z_T}\right) \quad (1.2.1)$$

where z_T is the top of the domain and z is the transformed coordinate at a point above the topography, η is the vertical coordinate on an empty mesh before it has been transformed and $h(x, y)$ is the height of the terrain. It is found that when using this coordinate system the effect of the terrain decreases linearly with height. This equation is for a Basic Terrain Following (BTF) mesh, and is similar to a type of terrain following coordinate known as sigma coordinates but does not use pressure. An example of a BTF coordinate is shown in figure 2a), from ***Schär et al 2002***. An alternative to BTF coordinates are Hybrid Terrain Following (HTF) coordinates where the effect of the terrain decreases exponentially with height (***Arakawa and Lamb 1977***) instead of linearly with BTF coordinates, as shown in figure 2b).

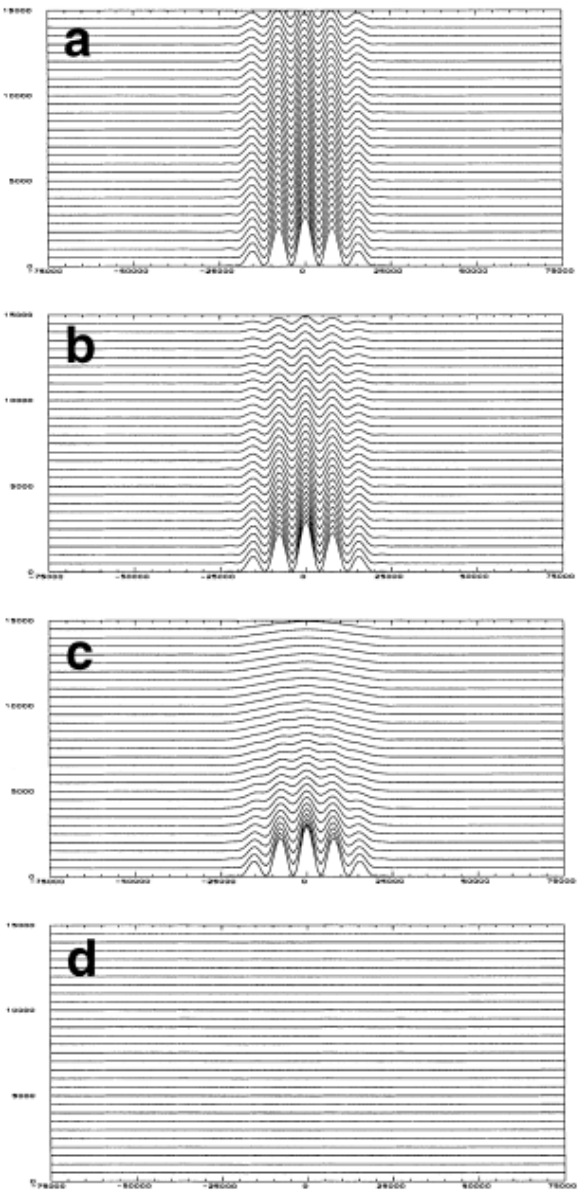

Figure 2 An image taken from Schär 2002 showing different terrain following meshes: a) Sigma mesh b) HTF mesh using scale height s = 8km c) SLEVE mesh using scale heights s1 = 15km s2 = 2.5km d) A reference grid with no topology

BTF and HTF coordinate meshes are characterised by their 'slow' decay of the terrain with height. SLEVE (Smooth Level Vertical) meshes, proposed in ***Schär 2000*** split the influence of the terrain on the mesh into two parts; a smooth representation of the terrain $h_1(x, y)$ and a representation which allows for more of the small scale features within the terrain $h_2(x, y)$ (***Leuenberger 2001***) thus leaving us with a z-coordinate on the Earth's surface given by equation 1.2.2.

$$h(x,y) = h_1(x,y) + h_2(x,y) \quad (1.2.2)$$

The coordinate transform for a SLEVE mesh is given in the following equation, where s_1 and s_2 are scale heights for the two z-coordinates above respectively.

$$z(x,y,\eta) = \eta + h_1(x,y)b_1(\eta) + h_2(x,y)b_2(\eta) \quad (1.2.3a)$$

$$b_i(\eta) = \frac{\sinh(\frac{H-\eta}{s_i})}{\sinh(\frac{H}{s_i})} \quad i = 1,2 \quad (1.2.3b)$$

Exp.	Coordinate	s_1	s_2	$\alpha_{1,inv}$	$\alpha_{2,inv}$	α_{inv}	Error
0	z	-	-	-	-	-	**0.023**
1	Gal-Chen	-	-	-	-	-	**0.350**
2	Exponential	6000 m	-	0.5	-	0.5	**0.120**
3	Exponential	3750 m	-	0.8	-	0.8	**0.037**
4	Exponential	3000 m	-	1.0	-	1.0	**0.027**
5	New	15000 m	3750 m	0.1	0.4	0.5	**0.061**
6	New	15000 m	2140 m	0.1	0.7	0.8	**0.025**
7	New	15000 m	1666 m	0.1	0.9	1.0	**0.024**
8	New	5000 m	2140 m	0.3	0.7	1.0	**0.023**

Table 1: A table from Leuenburger 2001, showing errors using different terrain following methods on a specfic test case. Run 0 uses z-coordinates (Used as a reference for other runs). Run 1 has the widely used Gal-Chen and Sommerville coordinates, Runs 2-4 Use HTF coordinates with varying resolution, runs 5-8 use SLEVE coordinates with varying resolution.

Here we find that the small scale features h_2 are able to rapidly decay with height, while the larger scale features decay more slowly. Figure 2 (***Schär et al 2002)*** gives a comparison of the different type of terrain following meshes, and most importantly, the decay of the influence of terrain with height, using the mountain from ***Schär et al 2002*** described in section 2.2 which is the mountain which shall be used in the experimental phase of this report.

The results from ***Schär et al. 2002***, were designed to show off the effect of two gravity waves forced by the orography. One using a broader scale, hydrostatic wave that is used to demonstrate deep vertical propagation and smaller scale waves caused by the cosine nature of the orography, used to demonstrate rapid decay with height due to non-hydrostatic effects. ***Leuenberger 2001***, also tested several terrain following coordinates using a 2D advection test and created an error parameter for each test by finding the difference in a

value ϕ between an analytical solution and the value given by each terrain following case. The results are given in table 1, and show that BTF coordinates are the least accurate with

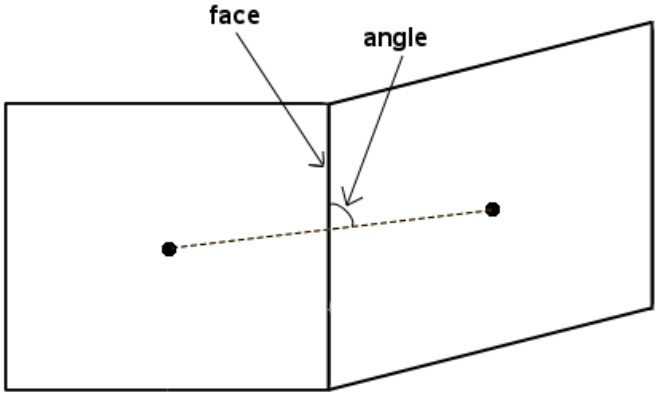

Figure 3: An image from Jones 2013, showing an example of two cells from a non-orthogonal grid

an error value of 0.350, HTF was slightly more accurate giving error value of around 0.027 and SLEVE was the most accurate with an error of 0.023.

Satomura 1989, tells us how it is more desirable to use an orthogonal grid than a non-orthogonal one to increase the accuracy of the output. If we look to implement

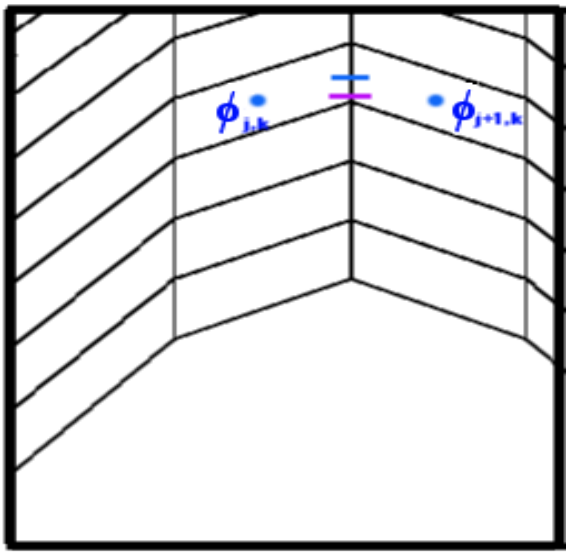

Figure 4: The two cells with centres ϕ_(j,k) and ϕ_(j+1,k) are orthogonal, but because the line between the two passes through the purple mark and not the blue mark there is an error caused by skewness (Jones 2013)

orthorgonality into a system, we have to look at specific grids rather than coordinates. The grid can be defined as orthogonal if the angle at the centre of two adjacent cells, and the cell wall is 90˚, as shown in figure 3 (**Jones 2013**). An orthogonal mesh, created in ***Jones***

2013 could also be tested for the case described in ***Schär et al 2002***, however this is beyond the scope of this report. Another problem can arise due to skewness between two cells. We find that two cells can be perfectly orthogonal, however there is an error in the skewness if the straight line between the centres of two cells does not cross the midpoint of the face between the two cells. An example of this is shown in figure 4 (***Jones 2013***). OpenFOAM, described in section 2.1, defines in its code that skewness is "Normalisation distance calculated as the approximate distance from the face in the direction of the skewness.". It is parameterised using

$$Skewness = \frac{|\boldsymbol{S_V}|}{f_d} \quad (1.2.4)$$

Where $\boldsymbol{S_V}$ is the displacement between the midpoint on the face between two cells and the point where the line between two cell centres crosses the face, and f_d is the distance between the midpoint of the same face and the top of the face.

1.3 An Idealised Advection Test to Quantify Errors in BTF and SLEVE coordinates

Originally in ***Schär et al 2002's*** an advection test was devised such that it would quantify errors in transformation to BTF and SLEVE coordinates. It should again be noted that sigma coordinates are similar to BTF coordinates, except it does not use pressure. The test had topography defined as:

$$h(x) = cos^2\left(\frac{\pi x}{\lambda}\right) h^*(x) \quad (1.3.1a)$$

where

$$h^*(x) = \begin{cases} h_0 cos^2\left(\frac{\pi x}{2a}\right) & for\ |x| \le a \\ 0 & for\ |x| \ge a \end{cases} \quad (1.3.1b)$$

In this case it was set up such that $a = 25km, h_0 = 3km$ and $\lambda = 8km$. Initial conditions for the wind profile were the set up so that the topography was lying completely within a stagnant pool of air near the ground using equation 2.4.2.

$$U(z) = U_0 \begin{cases} 1 & for\ z_2 \le z \\ sin^2\left(\frac{\pi}{2}\frac{z - z_1}{z_2 - z_1}\right) & for\ z_1 \le z \le z_2 \\ 0 & for\ z \le z_1 \end{cases} \quad (1.3.2)$$

where $U_0 = 10ms^{-1}$, $z_1 = 4km$ and $z_2 = 5km$. At $t_1 = 0s$, an anomaly is then assigned at a coordinate (x_0, z_0) this is clearly seen in figure 5 (***Schär et al 2002***) and has shape defined by the following equation.

$$\rho(x,z) = \rho_0 \begin{cases} cos^2\left(\frac{\pi r}{2}\right) & for\ r \leq 1 \\ 0 & otherwise \end{cases} \qquad (1.3.3a)$$

With

$$r = \left[\left(\frac{x - x_0}{A_x}\right)^2 + \left(\frac{z - z_0}{A_z}\right)^2\right]^{\frac{1}{2}} \qquad (1.3.3b)$$

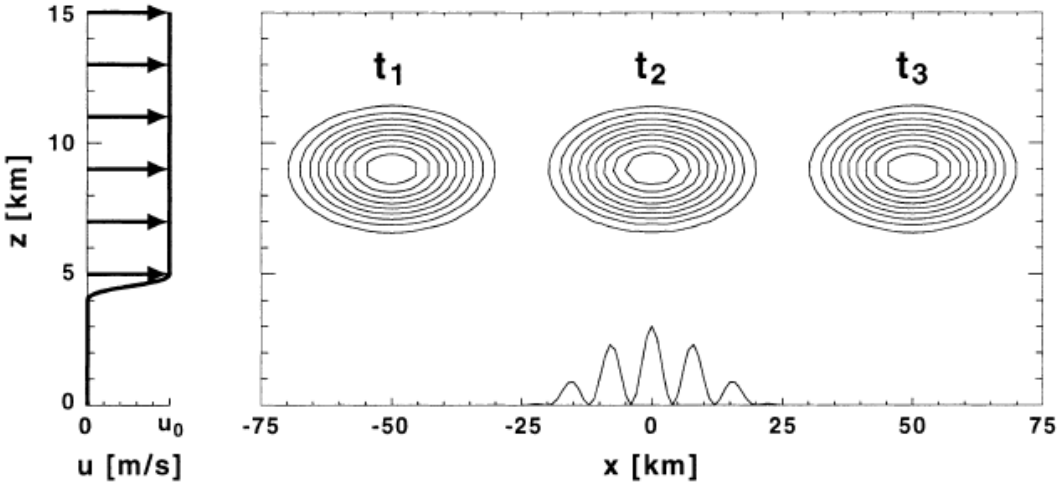

Figure 5: An analytical solution to the advection test from Schar et al 2002, showing the wind profile to the left, and the anomaly at three different time steps

If this anomaly is then advected using the fully compressible Euler equations (1.8.1 - 1.8.5) we find that after $t_2 = 2500s$ the anomaly should be centered directly above the orography and after $t_3 = 5000s$ the anomaly will be to the right of the orography and the advection is stopped. The test was then run using BTF and SLEVE coordinates, which can be seen labelled a) and c) in figure 2 respectively. The results to this advection test can be seen in figure 6, and they clearly show that the SLEVE coordinate mesh is much closer to the analytical solution than the sigma coordinate mesh. It should however be acknowledged that this advection test is likely to have been chosen to show that SLEVE is much more accurate than sigma coordinates, as when the paper was written SLEVE had only recently been formulated.

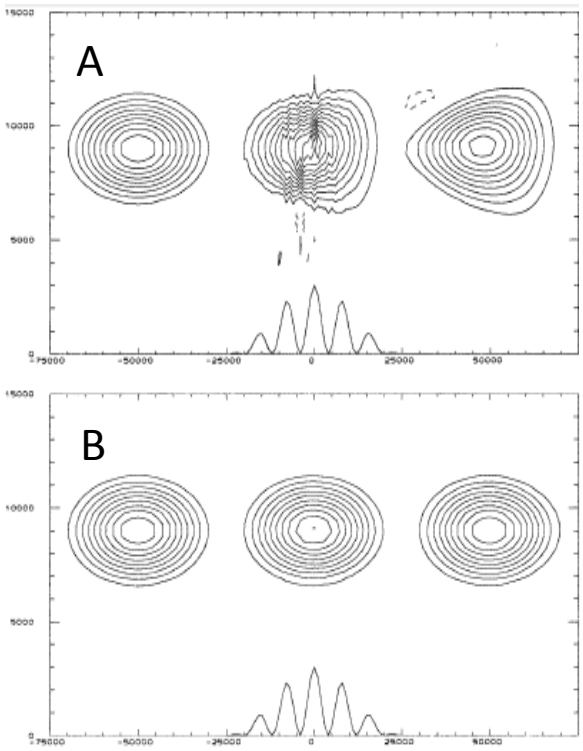

Figure 6: An image adapted from Schar et al 2002 showing the advection test, A using a sigma coordinate mesh, B using a SLEVE coordinate mesh

1.4 Step Orography

Another way of modelling over orography could be to use step-terrain vertical coordinate. This is where instead of using a coordinate transform, if part of the orography lies inside part of the cell then the mesh will 'step over' the orography. An example of this is shown in figure 10.

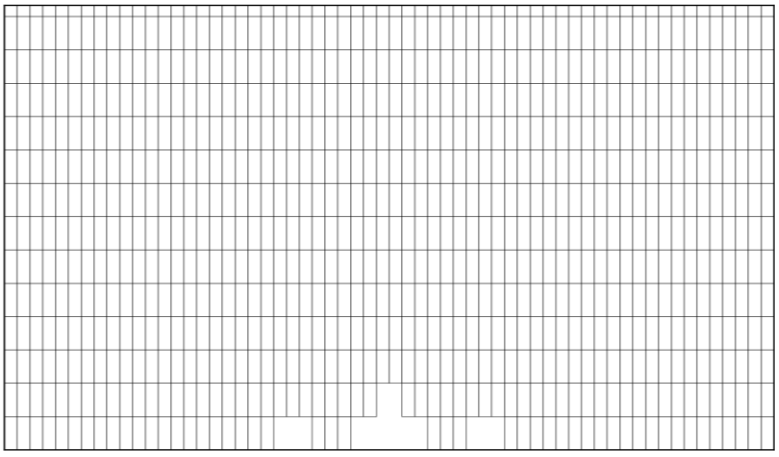

Figure 10: An example of Step Topography for the orography described in Schar et al 2002

Gallus and Klemp 2000 highlights a case where the Witch of Agnesi orography is tested using step-terrain coordinates. In this case the orography is described by equation 1.5.1:

$$h(x) = \frac{H}{1 + \frac{x^2}{a^2}} \qquad (1.4.1)$$

and the initial atmospheric conditions were set so that the Brunt–Väisälä frequency, N and wind speed U are constant with height. The results of this show that when using this type of representation of orography, the inviscid flow is not allowed to pass correctly down the Lee side of the slope. This type of coordinate will also be tested in this report using the ***Schär et al 2002*** orography, and compared to similar simulations for terrain following coordinates and cut cells.

1.5 The Finite Volume Method with Cut Cells

A cut cells method takes a different approach to modelling over orography. Here instead of following the terrain, when the cells reach the orography they become cut to fit the shape

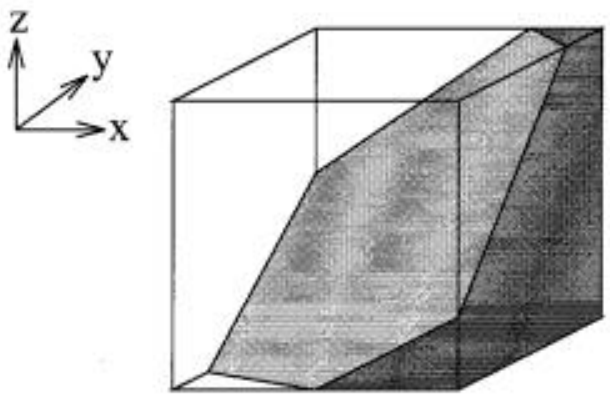

Figure 7: An example of a cell being cut by topography, taken from Adcroft et al 1997

of the orography. With the terrain following meshes, cells are transformed using an equation, such as 1.2.1 and 1.2.3, however with cut cells orography is implemented onto the mesh and cells are removed around the orography. Partial differential equations can be equated on a grid using the finite-volume method as described in ***Ferziger and Peric 2002***. A domain is split up into small cells, either using terrain following coordinates or cut cells, and each cell then has a control volume (CV) and is given a computational node at the centre of cell. This section will look at how we can model the flow through cut cells using the finite

volume method. Assuming we have a scalar variable ϕ which has a vector flux $\boldsymbol{F}$, we can write the conservation of ϕ can as equation 1.5.1:

$$\frac{\partial \phi}{\partial t} + \boldsymbol{\nabla}.\boldsymbol{F} = \mathrm{Q} \quad (1.5.1)$$

where Q are the sources of ϕ (***Adcroft et al 1997***). This equation can then be integrated over a fixed volume V with surface area A using Gauss' theorem, equation 1.5.2:

$$\int_V (\nabla \cdot \boldsymbol{F}) dV = \int_{\partial V} \boldsymbol{F} \cdot \boldsymbol{d}A$$

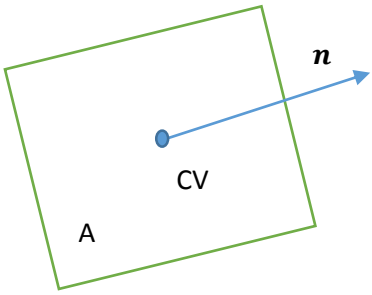

Figure 8: A cell with control volume CV at cell centre, with fixed area A and a vector n pointing perpendicularly away from the cell centre

then this leaves us with equation 1.4.3

$$\frac{\partial}{\partial t}\int_V \phi \, dV + \oint_A \boldsymbol{F}.\boldsymbol{d}A = \int_V Q \, dV \quad (1.5.3)$$

If we then let $\boldsymbol{dA} = \boldsymbol{n}A$ where $\boldsymbol{n}$ is a vector pointing away from a face with area A, we can write $\boldsymbol{F}$ in terms of ϕ and velocity $\boldsymbol{u}$ such that:

$$\boldsymbol{F} = \phi \boldsymbol{u}.\boldsymbol{n}A \quad (1.5.4)$$

We also know that our variable ϕ will vary in the volume V depending on the values of the flux $\boldsymbol{F}$ on the faces of the cells. We can then apply this equation to our discrete control Volume (CV) at the centre of each cell as follows:

$$V_i \frac{\partial \phi}{\partial t} + \sum_j F_{i,j} A_{i,j} = V_i Q_i \quad (1.5.5)$$

For any cell which is uncut, we can assume that the 6 walls of the cell will have boundary coordinates;

$$x = x_{i+\frac{1}{2}} \quad x = x_{i-\frac{1}{2}} \quad y = y_{j+\frac{1}{2}} \quad y = y_{j-\frac{1}{2}} \quad z = z_{k+\frac{1}{2}} \quad z = z_{k-\frac{1}{2}}$$

Where i, j and k are index values for each cell, in respective directions x, y and z. Therefore 1 single cell would have a volume, V of

$$V_{i,j,k} = \left(x_{i+\frac{1}{2}} - x_{i-\frac{1}{2}}\right)\left(y_{j+\frac{1}{2}} - y_{j-\frac{1}{2}}\right)\left(z_{k+\frac{1}{2}} - z_{k-\frac{1}{2}}\right) = \Delta x_i \Delta y_j \Delta z_k \quad (1.5.5)$$

For cut cells the volumes and cell areas must be calculated differently. Cut cells such as the one shown in figure 7, would have an integral produced to find the area of the cell which is

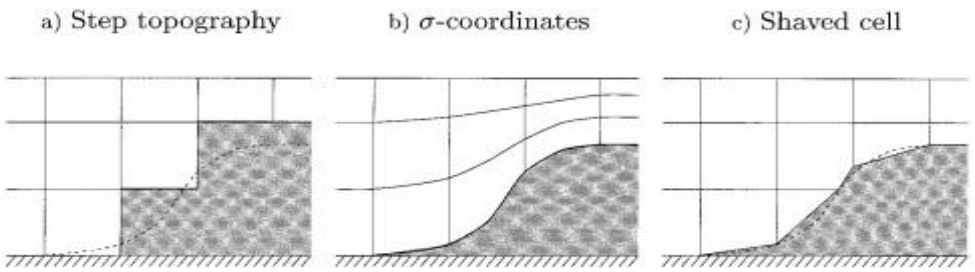

Figure 9: An image from Adcroft 1997, highlighting the differences between cut cell, sigma coordinate and Shaved Cell meshes

shaded and would then be subtracted from the total volume of a full cell given in equation (1.5.5). An example of a cut cell mesh is shown in figure 9c) (***Adcroft et al 1997***) and is compared with step topography 9a), described in section 1.4, and sigma coordinates 9b) a type of terrain following coordinate.

In ***Schär et al 2002's*** paper, an advection test is described to show the strengths of the SLEVE coordinate against other types of terrain following coordinates which lead to distortions of the advected tracer over the domain. It was found that SLEVE coordinates performed much better for this advection test than BTF coordinates. However in ***Good et al. 2014*****,** a similar advection test for cut cells proved just as good as SLEVE, which we would expect, as with cut cells there is no distortion in the mesh with height.

1.6 Analysis of Truncation Errors

Schär et al 2002, describes a detailed analysis of the truncation error before and after coordinate transformations. A truncation error can be defined as the difference between a function and it's series approximation when it is truncated up to a specific order of accuracy in computational space. The paper first describes the error associated with an upstream differencing scheme for the advection test described in section 1.3. The purpose of upstream differencing is to make hyperbolic partial differential equations easier to solve, using differences in the direction of the sign of characteristic speed (**Horton 1997**). For this scheme the truncation error is found to be of order $O(\Delta x)$. The equation for this difference scheme is given below:

$$f'(x_i) \approx \frac{f(x_{i+1}) - f(x_i)}{\Delta x} \qquad (1.6.1)$$

This was then compared with a centred differencing scheme where the difference between a value ahead of the current value x, and a value behind it is found and divided by Δx to find the derivative of the function. This is where an average of the forward and backward difference approximation schemes is found, and can be equated using equation 1.6.1.

$$f'(x_i) \approx \frac{f(x_{i+1}) - f(x_{i-1})}{2\Delta x} \qquad (1.6.2)$$

The centred differencing approximation truncation error for the advection test was found to be $O(\Delta x^2)$. The paper then continues to tell us that a Jacobian matrix used to transform the coordinates is the largest source of truncation error present on a uniform grid. We would expect the smallest errors therefore to be on grids which have the terrain decaying more smoothly with height, suggesting the SLEVE coordinate would have smaller errors than BTF coordinates.

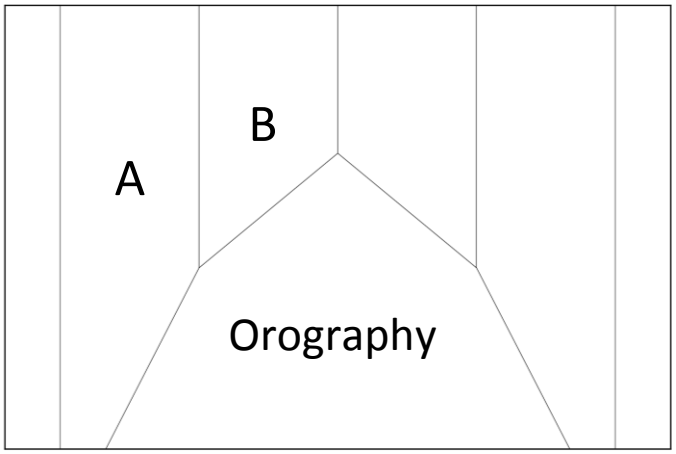

Figure 11: An image showing cut cells. Grids A and B are of different size, therefore we would expect the truncation error to be different between the two.

We would expect that there will be truncation errors within cut cells as well. Since the size of the cells within a cut cell approximation is not constant close to the terrain we would expect the truncation error to differ from cell to cell**. Burger et al 2013** tells us how cut cells can cause irregularities within the mesh which in turn causes non-smooth truncation errors at the walls between cells. Figure 11 shows a cut cell mesh with two cells, labelled A and B. They are clearly of different shape and size and we would expect that the truncation error to differ greatly between the two cells. The two other problems that would lead to truncation errors in these cells are non-orthogonality (***Eça 1998***), and skewness.

1.7 Small Cell Problems in Cut Cell Approximations

In ***Steppeler et al. 2002 and 2003***, a problem is described with Cut Cells when they become too small close to the terrain or a boundary. The paper describes how there are three cells in a cut cell mesh: those where the grids are below the Earth's surface, those that are completely above the topography, and those which become cut by the orography. A finite-volume method is then used, as described in section 1.4 to solve the equations of motion on

the mesh. Problems with small cells arise, due to the volume of cells being inversley proportional to the courant number, a measure of numerical instability (see section 2.3). So when the volume of a cell is very small, the instability can become very large.

In order to avoid the small cell problem, when OpenFOAM (see section 2.1) is used to create cut cells, if more than half the cell lies below the orography, that the grid lines will snap to a point on the topographic surface rather than continuing in a straight line, see figure 12. An example of this is used in this report and shows the importance of the regular cells when creating cut cells.

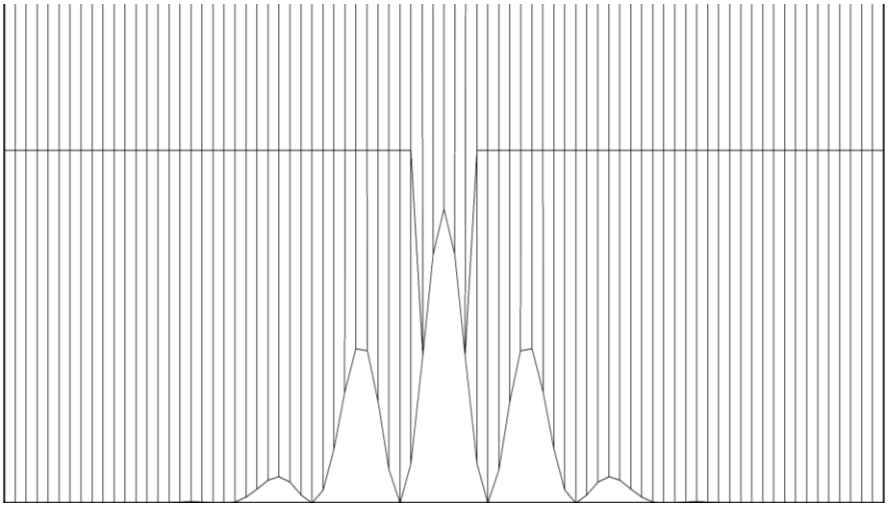

Figure 12: In order to avoid the small cell problem, small cells are combined with their nearest neighbour (shown above)

1.8 Fully Compressible Euler Equations

The fully compressible Euler equations will be solved on different types of terrain following and cut cell coordinates using the finite-volume method described in section 1.4. These are given in the equations below (***Weller and Shahrokhi 2014***):

$$Momentum: \quad \frac{\partial \rho \boldsymbol{u}}{\partial t} + \nabla \cdot \rho \boldsymbol{u}\boldsymbol{u} = \rho \boldsymbol{g} - \rho c_p \theta \nabla \Pi \qquad (1.8.1)$$

$$Continuity: \quad \frac{\partial \rho}{\partial t} + \nabla \cdot \rho \boldsymbol{u} = 0 \qquad (1.8.2)$$

$$Energy: \quad \frac{\partial \rho \theta}{\partial t} + \nabla \cdot \rho \boldsymbol{u} \theta = 0 \qquad (1.8.3)$$

$$State: \quad \Pi^{\frac{1-\kappa}{\kappa}} = \frac{R}{p_0}\rho\theta \qquad (1.8.4)$$

where ρ is density of the fluid, $\boldsymbol{u}$ is the wind speed vector, c_p is the specific heat capacity of air at constant pressure, t is time θ is potential temperature. It should also be noted that:

$$\theta = T\left(\frac{p}{p_0}\right)^{\kappa} \qquad (1.8.5a) \qquad \Pi = \left(\frac{p}{p_0}\right)^{\kappa} \qquad (1.8.5b)$$

where Π is the Exner function of pressure, p is pressure, p_0 is the surface pressure (typically 1000hPa) and κ is given below:

$$\kappa = \frac{R}{c_p} \qquad (1.8.6)$$

1.9 Dissertation Objectives

Within this dissertation I aim to:

- Reproduce the examples in ***Schär et al's 2002*** for the vertical velocity profiles using BTF and SLEVE terrain following coordinates
- Produce a cut cell mesh of the ***Schär et al 2002*** orography for this test case
- Produce a Step-Terrain mesh of the ***Schär et al 2002*** orography for this test case
- Increase the resolution of the mesh around the area where the mountain will be using a technique called local refinement
- Use some mesh relaxation techniques to create a combination of cut cells and terrain following coordinates

In the following section I will explain the methodology on how I expect to achieve the objectives which I have set above.

Methodology

2.1 OpenFOAM

During this project the C++ based free software package, OpenFOAM will be used to solve the fully compressible Euler equations (1.8.1 to 1.8.5). The software is able to solved partial differential equations on different types of structured and unstructured grids. Additional libraries were added to the software so that the equations could be solved and plotted on the meshes using Exner instead of pressure, equation 1.8.5b (***Weller and Shahrokhi 2014***).

2.2 The Test Case

The test case which will be used to simulate flow over orography using the different types of meshes will be from ***Schär et al 2002.*** The mountain is described by equation 2.2.1, and this is plotted in figure 13.

$$z(x) = h_m e^{-\left(\frac{x}{a}\right)^2} cos^2\left(\frac{\pi x}{\lambda}\right) \qquad (2.2.1)$$

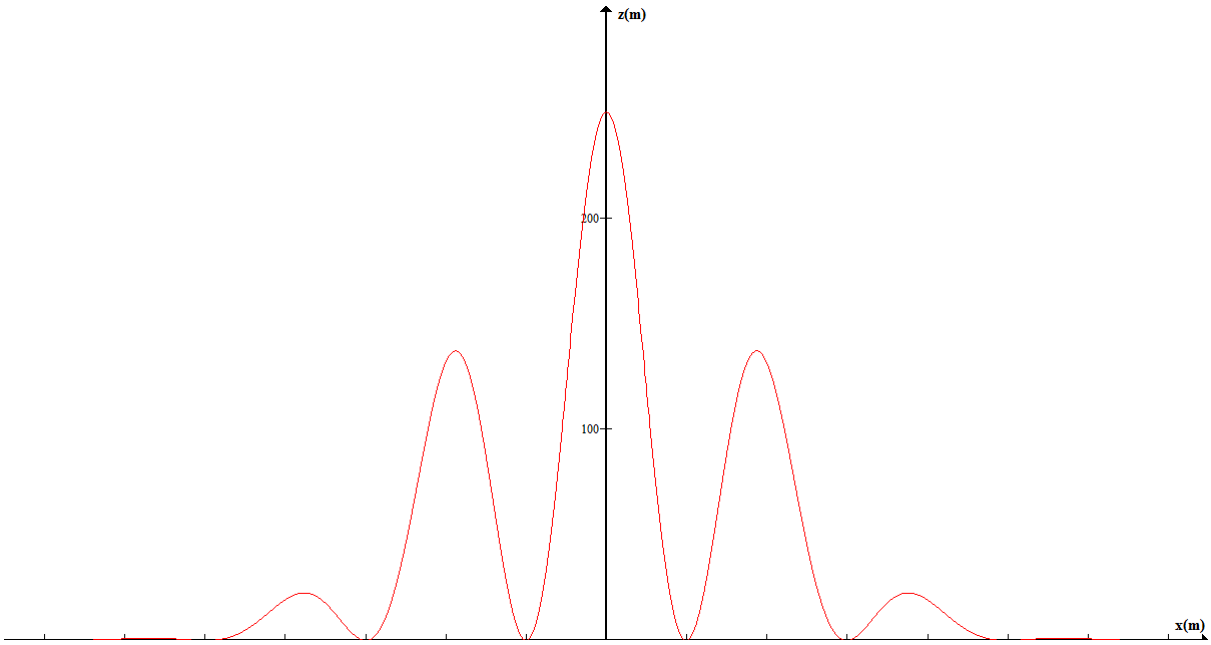

Figure 13: A graph representing the mountain to be used in this report, from Schär et al 2002

This test case was chosen in particular because it simulates flow that uses large scale and small scale features, making it particularly difficult for models to cope with as most terrain following methods struggle with small scale features (***Melvin et al 2010***). It also has not been tested before using cut cells, as most papers aim to show the benefits of cut cells by creating orography which cut cells are more likely to suit. It is speculated that one of the

reasons why this test case has not been used for cut cells is that for the resolutions given in the test case, the height of the first vertical gridline is above the orography, so none of the vertical grid lines can interact with the mountain. The orography was originally created to show the effectiveness of the SLEVE coordinate, which is split into two parts, where one works with small scale features, and the other the broader scale features. For this test case a background Brunt–Väisälä frequency, N of $0.01s^{-1}$ was applied and a mean wind speed U of $10ms^{-1}$.

2.3 The Courant Number

For a model to be stable, the one dimensional Courant Number (***Melvin et al. 2010***) described in equation 2.3.1 must remain small (usually less than 1):

$$C_x \equiv \frac{U\Delta t}{\Delta x} \qquad (2.3.1)$$

In more than one dimension, such as for the simulations that will be created within this report, we refer to equation 2.3.1 which OpenFOAM uses to create a variation of the Courant Number for unstructured grids.

$$C = \frac{\Sigma|\boldsymbol{u} \cdot d\boldsymbol{S}|}{V}\Delta t \qquad (2.3.2)$$

Where $\boldsymbol{u}$ is the velocity in a particular grid, $d\boldsymbol{S}$ is the surface vector for the grid, and V is the grid volume. (***OpenFOAM user guide***).

2.4 Reproducing Terrain Following Examples from the Literature

This section will describe how the terrain following examples used in ***Schär et al 2002's*** paper were reproduced. OpenFOAM was used to create a two dimensional blank mesh in the x, z plane with a domain with dimensions of 800km in the horizontal and 30km in the vertical, and the first examples had resolution $\Delta x = 500m$ and $\Delta z = 300m$. The mountain was then introduced to the mesh and the cells were shifted upwards using BTF coordinates using equation 1.2.1 and also SLEVE coordinates with equation 1.2.3.

However, once these grids are set up we then apply a sponge layer term introduced by (***Melvin et al. 2010***) which dampens the effect of reflections from the upper boundary of the domain. To apply the sponge layer we add a term to the momentum equation (1.7.1),

$-\mu\rho\boldsymbol{u}$ where μ is greater than 0 for values at the top of the domain. The sponge layer is described as:

$$\mu(z) = \begin{cases} 0 & for\ z < z_{sp} \\ \bar{\mu} sin^2\left(\frac{\Pi}{2}\frac{z - z_{sp}}{z_T - z_{sp}}\right) & for\ z \geq z_{sp} \end{cases} \quad (2.4.1)$$

Where z is a known height above the surface z_{sp} is the height of the sponge layer and z_T is the top of the domain. For this test case, also conducted by ***Melvin et al. 2010***, a time step of $\Delta t = 40s$ was used and that $\bar{\mu} = 33.\dot{3}$ and the height of the sponge layer is 20km. An initial condition for surface temperature of 288K is used. The top and bottom of the domain is fixed and has zero flux. A vertical θ profile was set throughout the domain to give N = $0.01s^{-1}$, and the profile for Π, the Exner Pressure, was set to be in hydrostatic balance.

A grid with half the vertical resolution, with $\Delta z = 600m$, was also created as a sensitivity study in order to alleviate the small cell problem in cut cells.

2.5 Creating Cut Cell and Step Orography Meshes For the Test Case

Similarly, the same domain and resolution described in section 2.4 was used for the cut cell mesh. There are two methods that could be used to create cut cells. We find that one snaps towards the mountain surface, so that cells are combined in order to alleviate the small cell problem. The alternative is an immersed boundary, where none of the internal mesh points are moved, shown in figure 16e). However, it is found that these immersed boundaries are non-orthogonal, which can causes problems with the accuracy of the output.

Using a variation of one of these methods, stair case (or Step) orography was also able to be created for the orography, shown in figure 18a). The resolution had to be increased on this case however as the terrain would have been completely lost otherwise. For this case a resolution of $\Delta x = 500m$ and $\Delta z = 150m$ was used.

2.6 Introducing Local Refinement to the Cases

As discussed previously, one of the key features of modelling the atmosphere is the decreasing of resolution with height so that the bottom of the domain can be modelled in the greatest detail. However with high orography, we find that the top of the mountain can be above the highest resolutions. To replicate this local refinement was introduced into some of the test cases. A box was put over the orography was put into the domain with dimensions of 12000m in the x direction and 600m in the z direction. The resolution within this box was $\Delta x = 62.5m$ and $\Delta z = 300m$ with a background resolution of $\Delta x = 500m$ and $\Delta z = 600m$. BTF, SLEVE and Cut Cells were then introduced to the mesh as described above for the ***Schar et al. 2002*** test case.

2.7 Using Relaxation Methods to Combine Cut Cells and Terrain Following Coordinates

One of the advantages of using OpenFOAM is that relaxation techniques can be applied to the mesh. This can act as another way of alleviating the small cell problem with cut cells, and by increasing the number of relaxation iterations on the mesh, the way in which grid lines are snapped to the mesh becomes much smoother than the method previously described. A side effect of this is that the lower most vertical gridlines are forced to follow the shape of the terrain similarly to that of terrain following coordinates.

Figures 18e) and 18f) show two examples which were created using this method. 18e) has a background resolution $\Delta x = 500m$ and $\Delta z = 300m$, with a locally refined region in the same region within the mesh as described in the previous section, with a very high resolution of $\Delta x = 500m$ and $\Delta z = 18.75m$. This was in order to test whether dramatically increasing the resolution close to the bottom of the domain could significantly increase the accuracy of the results. 18f) was simply a mesh with resolution $\Delta x = 500m$ and $\Delta z = 150m$, and the purpose of this mesh was to have cut cells which had the first vertical gridline below the maximum height of the mountain.

Results

This section shows the results for the test case on various different meshes. The following section will provide a discussion and analysis of these results.

3.0 Tables and Figures

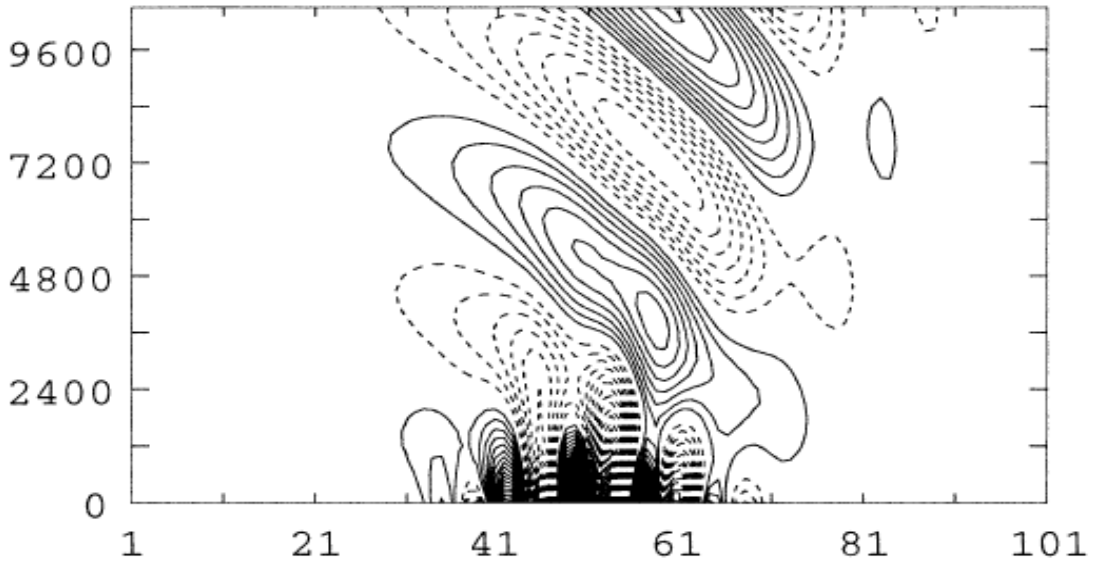

Figure 14: An Analytical Solution to the Test Case from Schär et al 2002 to be used as a reference for remaining results. This solution was created by solving linearised equations and therefore we would expect the following results which solve non-linear equations not to be exactly the same as this solution. Note that the $x$scale is in km, whilst the z scale is in m.

Type	nxm	n. cells	Δx		Δz		Max skewness	Non orthorgonality		Δt
			Min	Mx	Min	Mx		Max	Avg	
SLEVE	800x 50	40000	500		100	611	0.202	9.23	0.174	40
SLEVE	800x 100	80000	500		56.3	306	0.130	9.73	0.180	40
BTF	800x 50	40000	500		600		0.209	10.03	0.444	40
BTF	800x 100	80000	500		300		0.130	10.18	0.446	40
Cut Cells	800x 50	40000	500		600		0.185	8.90	0.074	40
Cut Cells	800x 100	80000	500		300		0.097	7.33	0.053	40
SLEVE LR	800x 50	40144	250	500	300	600	0.340	24.4	0.629	40
BTF LR	800x 50	40144	250	500	300	600	0.339	25.7	0.754	40
Cut Cells LR	800x 50	40144	250	500	300	600	0.334	21.8	0.564	40
Small Cell Sol'n	800x 100	80000	500		300		0.275	5.82	0.057	40
Step	800x 200	160000	500		150		0	0	0	8

Table 2: A table summarising the properties of the different meshes which were tested, where nxm is the number of grids in the x, z direction, and n. cells is the total number of cells. Note that LR stands for localised resolution.

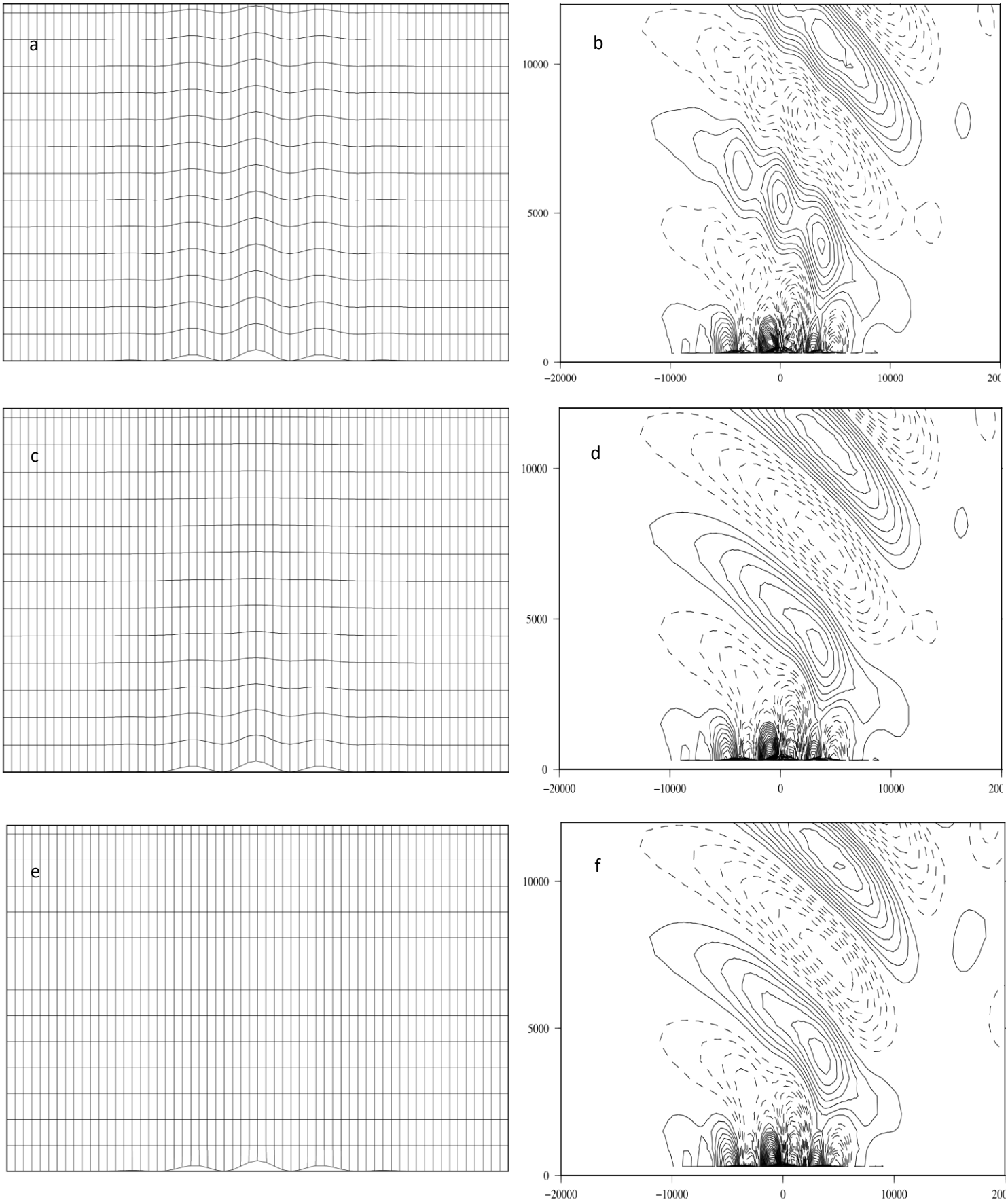

Figure 15: A figure to show the different types of mesh created with resolution Δx=125m, Δz=600m and the vertical velocity profile after 5 hours using the test case from Schär et al. 2002 with initial conditions N = 0.01s^{-1} and U =10m/s. Figures a+b are for BTF coordinates, c + d are for SLEVE coordinates and e + f for cut cells. Vertical velocity contours are at intervals of 0.05ms^{-1}, where black lines are positive values and dashed lines are negative values.

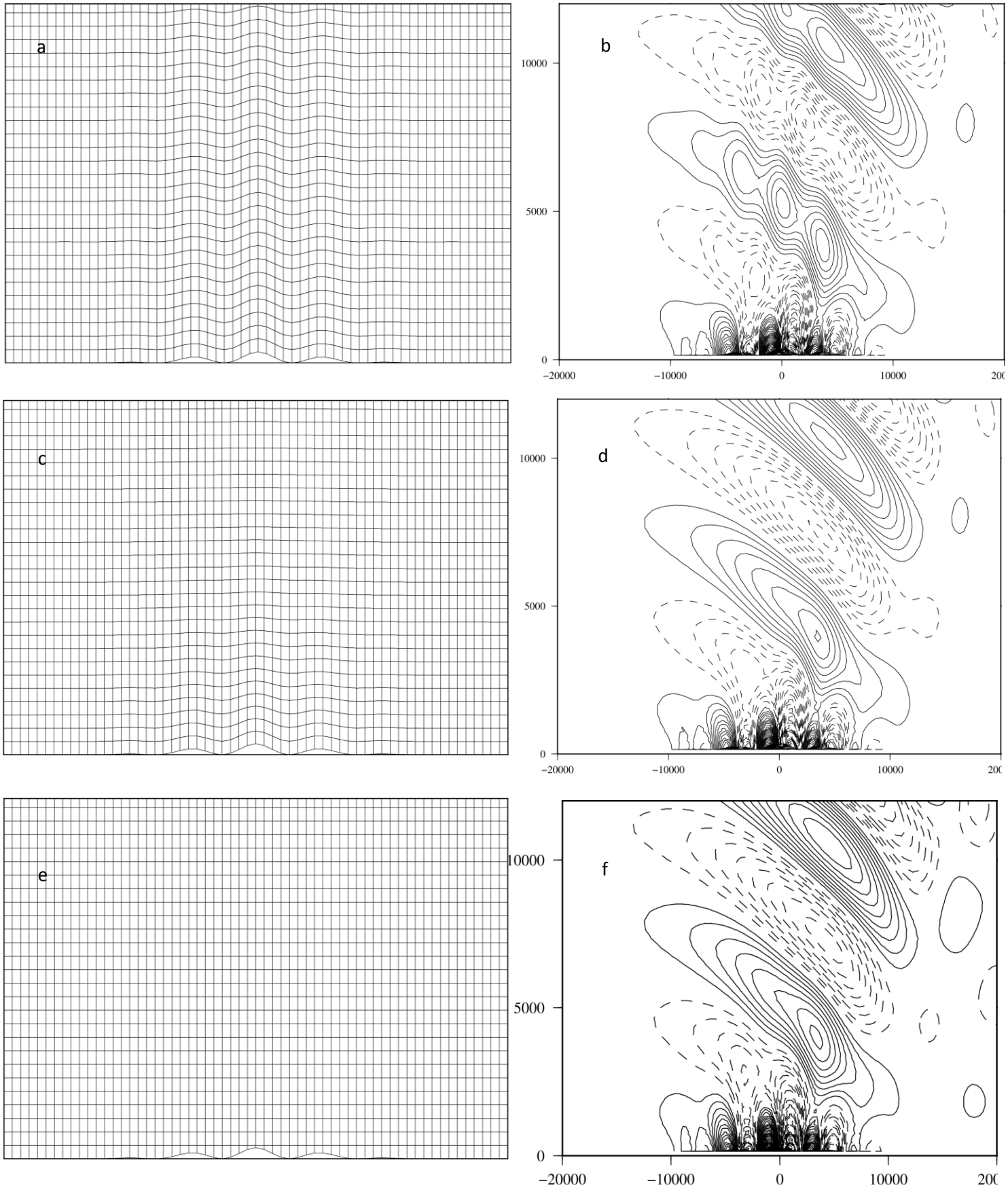

Figure 16: A figure to show the different types of mesh created with resolution Δx=125m, Δz=300m and the vertical velocity profile after 5 hours using the test case from Schär et al. 2002 with initial conditions N = 0.01s^{-1} and U =10m/s. Figures a+b are for BTF coordinates, c + d are for SLEVE coordinates and e + f for cut cells. Vertical velocity contours are at intervals of 0.05ms^{-1}, where black lines are positive values and dashed lines are negative values.

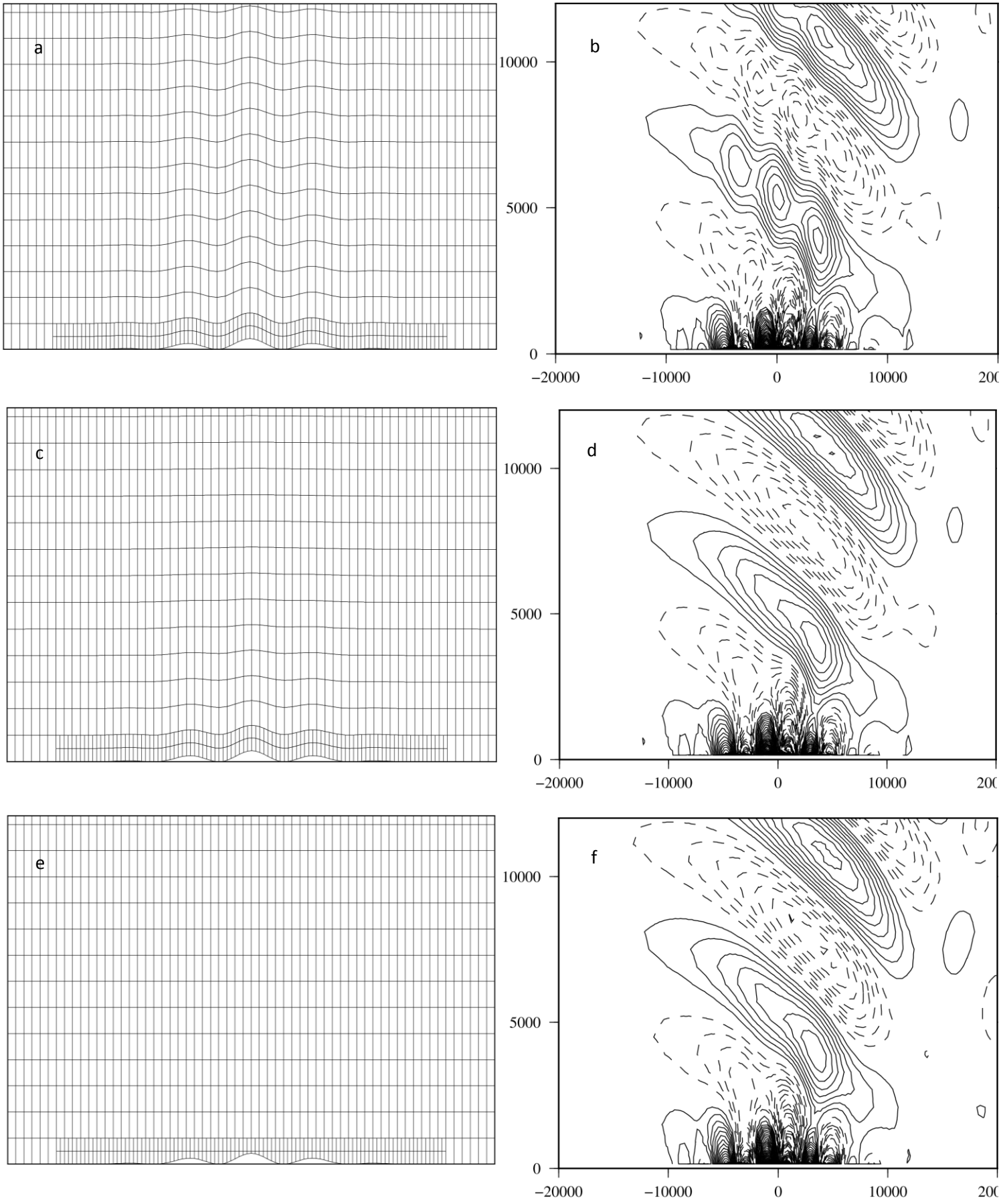

Figure 17: A figure to show the different types of mesh created with background resolution Δx=500m, Δz=600m and resolution in a box close to the orography of Δx=250m, Δz=300m. The vertical velocity profile is also shown after 5 hours using the test case from Schär et al. 2002 with initial conditions N = 0.01s^{-1} and U =10m/s. Figures a+b are for BTF coordinates, c + d are for sigma coordinates and e + f for cut cells. Vertical velocity contours are at intervals of 0.05ms^{-1}, where black lines are positive values and dashed lines are negative values.

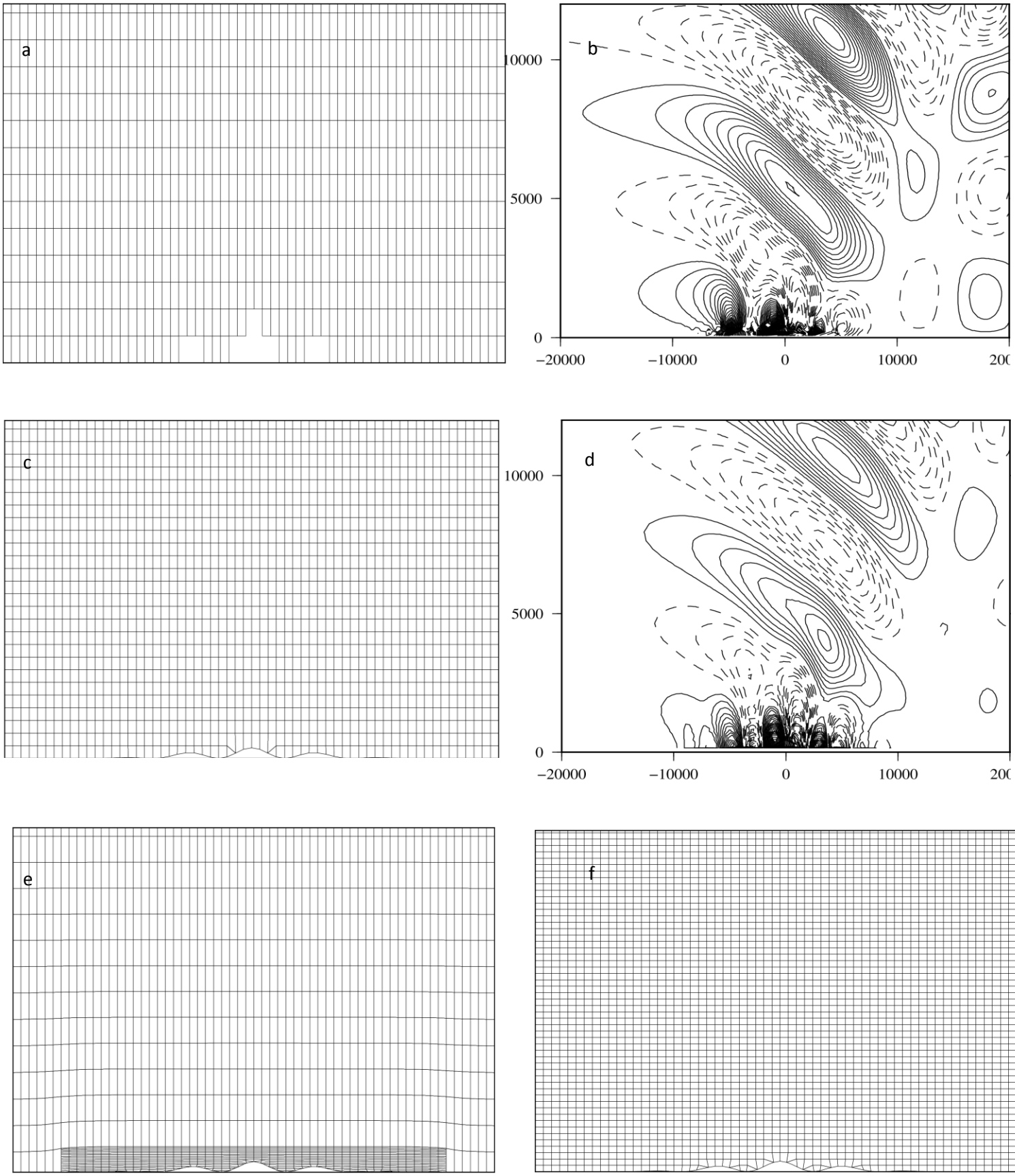

Figure 18: Parts a+b show the Schar et al 2002 orography being tested using Step Orography with resolution Δx=125m, Δz=150m and the vertical velocity profile after 5 hours. Parts c+d show OpenFOAM's solution to the small cell problem where small cell faces are snapped to their nearest neighbour with the same resolution of parts e+f of figure 17. Parts e+f show two meshes which have used relaxation techniques which cause cells to become cut as well as terrain following.

3.1 The Terrain Following Cases

Figures 15b) and 16b) show the vertical velocities with separation $0.05m\ s^{-1}$ for the BTF coordinates with vertical resolutions $\Delta z = 600m$ and $\Delta z = 300m$ respectively, with horizontal resolution $\Delta x = 500m$ for both cases. Figures 15d) and 16d), show the results for SLEVE using the same resolutions. All simulations were run with a time step, $\Delta t = 40s$. To the left of all these results are the corresponding meshes which they were run on. It is found that similarly to ***Schär et al 2002's*** results for BTF and SLEVE coordinates, these results show that the SLEVE case is much closer to the analytical solution than the BTF coordinates. The results show that for the BTF coordinates that using both resolutions, the vertical velocity directly above the orography becomes distorted whilst the SLEVE coordinates keep a much smoother profile of velocity. It can be noted that when the vertical resolution is increased we see that a downdraft close the coordinate $x = +9000m, z = 0m$ is modelled, whereas this is not evident on the lower vertical resolution, and that this is the same for both BTF and SLEVE.

3.2 The Cut Cell Cases

Figures 15f) and 16f) show the results for cut cells with vertical resolutions of $\Delta z = 600m$ and $\Delta z = 300m$ respectively, with horizontal resolution $\Delta x = 500m$ for both cases. This test had not previously been done in the literature as the first horizontal grid line lies above the orography, and this particular orography had been designed for SLEVE coordinates. At first glance the differences in results between the SLEVE and cut cells vertical velocity profiles seem small. In the lower vertical resolution however, cut cells produce 9 positive vertical velocity contours in the uppermost wave, whereas SLEVE only produces 8. This can then be compared with the analytical solution, figure 14, which also produces 9 positive contours, so we could say that cut cells have been more accurate at lower resolutions. However, to the right of the orography cut cells produces some isolated contours, both positive and negative, which simply don't appear on the SLEVE results or in fact the analytical solution.

The following figure (figure 19) allows us to look at another perspective on the difference between SLEVE and cut cells.

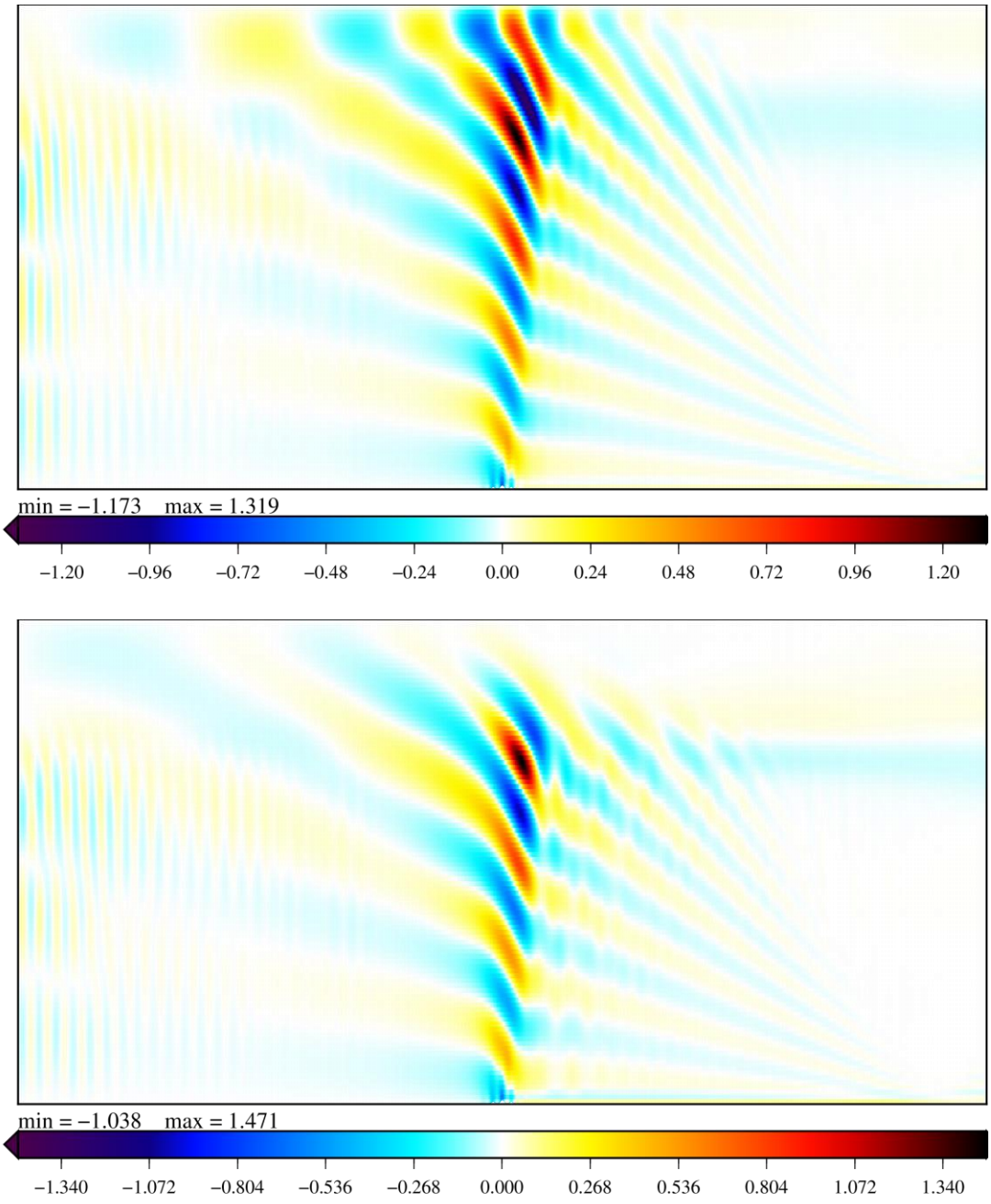

Figure 19: A figure showing the differences in potential temperature, θ (K), from the initial conditions to 5 hours after running, for firstly SLEVE coordinates, and secondly cut cells.

The figure allows us to see how the potential temperature has changed over the 5 hours for SLEVE coordinates and cut cells. The figure also shows the whole domain, i.e. 800km in the x-direction and 30km in the z-direction. We can see that the magnitude of these values for SLEVE is much larger at the top of the domain than cut cells, which is denoted by the more intense red and blue colours within the first image. Both images show a gravity wave

structure to the right of the orography, however the structure within the cut cells results (the second image), shows that this wave is much more distorted than with the SLEVE results. This could be indicative of why strange contours of vertical velocity are appearing on the right hand side of the domain for cut cells.

One final point that should be noted for cut cells, is that when the resolution is increased, similarly to the terrain following examples a downdraft begins to appear close to the coordinate $x = +9000m, z = 0m$, showing the improved accuracy due to an increase in resolution.

3.3 OpenFOAM's solution to the small cell problem in Cut Cells

When cell volumes become very small, the courant number can become too large causing numerical instability. An example of OpenFOAM's solution to the small cell problem in cut cells is shown in figure 18c) with the resulting vertical velocity profile after 5 hours shown in figure 18d). The resolution of this mesh was $\Delta x = 500m$ and $\Delta z = 300m$, and therefore can be compared to figures 16e) and 16f) which use the same method however when cells are small they do not snap to their nearest neighbour. On first observations it is surprising how well the results have materialised. It was expected that due to the large non-orthorgonality of the cells which have snapped to their nearest neighbour that the results would seriously overestimate or underestimate the magnitude of the vertical velocity. However when compared with the original cut cell results at this resolution it is found that the results are very similar, with only some slight problems in the quality of the velocity profile close to the terrain being the only major difference between the two profiles.

3.4 Local Refinement of the different Cases

The examples on figure 17 all show cases of local refinement for BTF coordinates, SLEVE coordinates and Cut Cells respectively. The background resolution here is $\Delta x = 500m$ and $\Delta z = 600m$, with a local resolution at the bottom 600m of the domain of $\Delta x = 250m$ and $\Delta z = 300m$. As expected for all three cases the accuracy of the vertical velocity profile close to the orography is increased by implementing this method when comparing with the examples in figure 15 where the resolution is $\Delta x = 500m$ and $\Delta z = 600m$ and is constant throughout the domain. This is due to the appearance of the downdraft at coordinates $x = +9000m, z = 0m$, which previously only appeared in the higher resolution case, but now appears in the locally refined case. However we find that away from the orography, higher

up in the atmosphere that the vertical velocity profile is still not as smooth and more like the low resolution results. These results are pleasing however, as it allows us to produce higher resolution results with just a fraction of the computational cost that it would using high resolution for the whole domain.

3.5 The Step Orography Case

Figure 18a) shows a step orography mesh with the subsequent result for this test case. Here a resolution of $\Delta x = 500m$ and $\Delta z = 150m$, with a time step $\Delta t = 8s$ was used. A higher vertical resolution than previous Terrain Following and Cut Cell meshes had to be used, or the orography would become lost within the mesh. This is clearly the least accurate of all the results. It can first be noted that the magnitude of the vertical velocity is significantly overestimated above the orography, and many closed contours of velocity are created on the right hand side of the domain which don't appear in the analytical solution. We would expect that these errors are due to a failure within Step Orography that it does not allow inviscid flow to correctly pass down the lee side of orography, as described in ***Gallus and Klemp 2000***. Another problem with this is that step orography has sharp vertices, which causes the velocity to rise upwards much more unnaturally than it would do otherwise. This may explain why the vertical velocity profile is poor close to the lee side of the orography, and why closed contours of velocity are incorrectly created to the right hand side of the domain.

3.6 Problems with the Relaxation Techniques

Figures 18e) and 18f) show the two meshes that were created using the mesh relaxation techniques. Unfortunately when the Euler equations (equations 1.8.1-1.8.4) were solved for this mesh, the results diverged after just one time step. This was surprising, as at first it was expected that if the numerical method which was used, worked on the local refinement cases, then it was assumed that it would also work for the cases where relaxation techniques had been used. It is speculated that due to the irregular shape of some of the cells in 18e) and 18f), that it could be this which is preventing the numerical method from working. Further work is needed to understand what is causing this instability, however unfortunately it is beyond the scope of this report.

Conclusions

4.1 Conclusions of Results

From this report we can conclude that SLEVE coordinates are currently the best way to represent to the vertical profile over the orography first described in ***Schär et al 2002*.** This is contrary to arguments in the literature that cut cells are the most accurate way of representing orography. It should however be noted that this particular orography was designed to show the benefits of SLEVE coordinates, particularly how they can cope with smaller scale features within the orography. The reason that the BTF coordinates in this report are less accurate than that of ***Weller and Shahrokhi 2014***, is mostly down the fact the advection scheme in this report assumes there is no skewness between cells, whereas the improved method does account for this. Therefore for the results shown in figures 15b) and 16b) the cell to cell cross over point is assumed to be at the cell centre, whereas the BTF coordinates in ***Weller and Shahrokhi 2014*** use a more expensive scheme that do not make this assumption. If these BTF coordinates had been used instead, the distortion of the vertical velocity profile above the orography would not have been evident.

Cut cells were likely to struggle with this particular test case as the resolution causes the first horizontal coordinates to be above the maximum height of the orography, however there are only small differences between the cut cell results and SLEVE results when compared with the analytical solution, and cut cells appear to be slightly more accurate closer to the terrain. It could be concluded that on most types of orography cut cells are better in terms of accuracy of results, however when small scale features dominate the shape of the orography then it may be wiser to use SLEVE coordinates. Table 2 shows that cut cells have smaller levels of non-orthorgonality and skewness than the terrain following examples. It shows that for the lower resolution meshes that cut cells have an average non-orthorgonality of 0.074, whereas SLEVE has a value of 0.174 and BTF coordinates a value of 0.444. Similarly, the cut cell mesh has a maximum skewness value of 0.185, whereas SLEVE has a maximum value of 0.202 and BTF is 0.209 which again would contribute to a smaller error with cut cells than our terrain following results. These two factors are two of the things which can reduce the accuracy, so the fact that cut cells have smaller values for both, than terrain following coordinates shows that in general we may expect the cut cells

technique to be more accurate than terrain following coordinates. Again it shows for this test case, that SLEVE produces more accurate results largely because it was designed to cope with the small features of this orography. We can also deduce from our results that step orography does not perform will with this type of orography. Step orography is the most basic way in which we can model the atmosphere over orography, and in this case it is simply too complex to be modelled in this way.

It can also be speculated that the numerical method used to solve the Euler equations of motion (equations 1.8.1 to 1.8.4) cannot be used for irregular cells. Due to this problem it meant that meshes created in OpenFOAM with relaxations were not able to be solved as they diverged after one time step.

Techniques designed to solve the small cell problem, such as combining cells, can lead to much larger mesh distortions than those introduced by terrain following coordinates. In contrast, local refinement of orography introduces no obvious errors in the solution, and was in fact beneficial, as it introduces a downdraft around coordinate $x = +9000m, z = 0m$.

4.2 Possible Future Work

In the future it could be possible to create terrain following and cut cell grids using orthogonal meshes, such as in ***Jones 2013***. These could then been compared to see if they reduce errors in the numerical output of modelling over steep orography, and whether a cut cells approach is still more accurate than a terrain following coordinates. BTF coordinates with the advection test used in ***Weller and Shahrokhi 2014*** to show that the accuracy of these coordinates can be increased when used on the ***Schär et al 2002*** test case. The numerical method used could be adapted to run on irregular grids instead of diverging after one time step, allowing the relaxed meshes which were created in this report to be tested again. An error parameter could also be designed in a similar way to that of ***Leuenberger 2001*** (see table 1), where he created an error value by finding the difference in a value ϕ and an analytical solution for each case he created. It is difficult to do for this case, as our results are created by solving non-linear equations, whereas Leuenberger had linearised equations. This would make it much easier to see which method is more accurate than just looking at the results for the vertical velocities and comparing it to the analytical solution

visually. It would involve creating our own analytical solution however, as we would need to produce the solution using the same software as our meshes have been created.

The horizontal resolution could also be halved, instead of just the vertical resolution being halved. This would keep the ratio of vertical to horizontal resolutions, which may have in this case affected the accuracy of the results. Also, an even coarser resolution could be tested to see if there were any more obvious inaccuracies. By increasing the height of the orography, so that the first horizontal gridline was below the maximum height, this would increase the relevance of cut cells for this particular orography with small scale and larger scale gravity waves.

Acknowledgement

I would like to thank Dr Hilary Weller, for the large amount of time and work she has put into helping me with this dissertation for which I am extremely grateful.

References

Adcroft, A., C. Hill, and J. Marshall, 1997: Representation of topography by shaved cells in a height coordinate ocean model. Mon. Wea. Rev., 2293-2315.

Arakawa, A., Computational design of the basic dynamical processes of the UCLA general circulation model, Methods in Computational Physics, 17, 173–265, 1977.

Eça, L., 1998: Orthogonal generation systems. Handbook of Grid Generation, J. F. Thompson, B. K. Soni, and N. P. Weatherill, Eds., CRC Press, Chapter 7.

Ferziger, J. H., and Perić, M., 2002: Finite Volume Methods*. Computational Methods for Fluid Dynamics. Springer. pp 71-82.*

Gal-Chen, T., and R. Somerville, 1975: On the use of a coordinate transformation for the solution of the Navier-Stokes equations.J. Comput. Phys., 17, 209–228.

Gallas, W., Klemp, J. B., 2000: Behavior of Flow over Step Orography. Mon. Wea. Rev., 1153-1164.

Good, B., Gadian, A., Lock, S. J., Ross, A., 2014: Performance of the cut-cell method of representing orography in idealized simulations. R. Met. Soc. 44-49.

Harten, A., Lax, P. D., Van Leer, B., 1997: On Upstream Differencing and Gudunov-Type Schemes For Hyperbolic Conservation Laws. Springer-Verlag. Berlin.

Ingram, D. M., Causon, D. M., and Mingham, C. G., 2003: Developments in Cartesian cut cell methods. Els. Sci. B.V, 561-572.

Jones, M., 2013: Vertical Coordinates over Orography. Univ. of. Rea.

Klemp, J. B., 2011: A terrain-following coordinate with smoothed coordinate surfaces. Mon. Wea. Rev., July 2011, 2163-2169.

Leuenberger, D., 2001: A New Terrain-Following Coordinate for High-Resolution Atmospheric Models.

Melvin, T., Dubal, M., Wood, N., Staniforth, A., and Zerroukat, M., 2010: An inherently mass-conserving iterative semi-implicit semi-Lagrangian discretization of the non-hydrostatic vertical-slice equations. Q. J. R. Meteorol. Soc. 136: 799–814, April 2010

OpenFOAM User's Guide, 2013: OpenFOAM, the Open Source CFD Toolbox, User's Guide, version 2.2.2. OpenFOAM.

Satomura, T., 1989: Compressible Flow Simulations on Numerically Generated Grids. Jou. Met. Soc. Jap., 473-481.

Schär, C., A generalized vertical coordinate for high-resolution NWP models, pp. 1–5, 2000a.

Schär, C., D. Leuenberger, O. Fuhrer, D. Leuthi, and C. Girard, 2002: A new terrain-following vertical coordinate formulation for atmospheric prediction models. Mon. Wea. Rev., October 2002, 2459-2480.

Steppeler, J., Park, S. H., and Dobler, A., 2013: Forecasts covering one month using a cut-cell model. Geo. Mod. Dev., 875-882.

J. Steppeler, H. Bitzer, M. Minotte, and L. Bonaventura. Non-hydrostatic atmospheric modelling using a z-coordinate representation. Mon. Wea. Rev., 130(8):2143–2149, 2002

J. Steppeler, R. Hess, U. Schattler, and L. Bonaventura. Review of numerical methods for non-hydrostatic weather prediciton models. Meteorology and Atmospheric Physics, 82(1-4):287–301, 2003

Weller, H., and Shahrokhi, A., 2014: Curl-free pressure gradients over orography in a solution of the fully compressible Euler equations with long time-steps. Amer. Met. Soc.